bioRxiv preprint doi: https://doi.org/10.1101/665570; this version posted June 11, 2019. The copyright holder for this preprint (which was not certified by peer review) is the author/funder, who has granted bioRxiv a license to display the preprint in perpetuity. It is made available under aCC-BY 4.0 International license.

LSF small molecule inhibitors phenocopy LSF-targeted siRNAs causing mitotic defects and senescence in cancer cells

Jennifer L.S. Willoughby[1,2], Kelly George[3], Mark P. Roberto[2], Hang Gyeong Chin[4,5], Patrick Stoiber[2,4], Hyunjin Shin[6], Chandra Sekhar Pedamallu[7,8], Scott E. Schaus[9], Kevin Fitzgerald[1], Jagesh Shah[3] and Ulla Hansen[2,4]*

[1]Alnylam Pharmaceuticals, Inc., Cambridge, MA 02142

[2]Department of Biology, Boston University, Boston, MA 02215

[3]Department of Systems Biology, Harvard Medical School, Boston, MA 02115

[4]MCBB Graduate Program, Boston University, Boston, MA 02215

[5]New England BioLabs, Ipswich, MA 01938

[6]Data Science Institute, Takeda Pharmaceuticals International, Inc., Cambridge, MA 02139

[7]Broad Institute of Massachusetts Institute of Technology and Harvard, Cambridge, MA 02142

[8]Department of Medical Oncology, Dana-Farber Cancer Institute and Harvard Medical School, Boston, MA, 02115

[9]Center for Molecular Discovery, Department of Chemistry, Boston University, Boston, MA 02215

Running Title: LSF inhibition causes mitotic defects and senescence

Keywords: LSF, FQI1, siRNA, mitosis, senescence

***Corresponding Author:** Ulla Hansen, Ph.D., E-mail:uhansen@bu.edu, Phone: (617) 353-8730, FAX: (617) 353-8484; Department of Biology, Boston University, 5 Cummington Mall, Boston, MA 02215, USA.

Financial Support: The research was supported by: Alnylam Pharmaceuticals, Inc (JLSW, KF), Boston University (JLSW, UH, SES), BU Undergraduate Research Opportunity (MR), New England Biolabs, Inc. (HGC), and the NIH (R01 GM078240) to SES.

Conflict of Interest Disclosure: SES and UH are co-founders of Lamerigen, Inc. JLSW and KF are employed by Alnylam Pharmaceuticals. The remaining authors declare no potential conflict of interest.

bioRxiv preprint doi: https://doi.org/10.1101/665570; this version posted June 11, 2019. The copyright holder for this preprint (which was not certified by peer review) is the author/funder, who has granted bioRxiv a license to display the preprint in perpetuity. It is made available under aCC-BY 4.0 International license.

Abstract

The oncogene LSF has been proposed as a novel target with therapeutic potential for multiple cancers. LSF overexpression correlates with poor prognosis for both liver and colorectal cancers, for which there are currently limited therapeutic treatment options. In particular, molecularly targeted therapies for hepatocellular carcinoma targeting cellular receptors and kinases have yielded disappointing clinical results, providing an urgency for targeting distinct mechanisms. LSF small molecule inhibitors, Factor Quinolinone Inhibitors (FQIs), have exhibited robust anti-tumor activity in multiple pre-clinical models of hepatocellular carcinoma, with no observable toxicity. To understand how the inhibitors impact cancer cell proliferation, we characterized the cellular phenotypes that result from loss of LSF activity. Phenotypically, inhibition of LSF activity induced a mitotic delay with condensed, but unaligned, chromosomes. This mitotic disruption resulted in improper cellular division leading to multiple outcomes: multi-nucleation, apoptosis, and cellular senescence. The cellular phenotypes observed upon FQI1 treatment were due specifically to the loss of LSF activity, as siRNA specifically targeting LSF produced nearly identical phenotypes. Taken together, these findings confirm that LSF is a promising therapeutic target for cancer treatment.

Significance Specific inhibition of LSF by either small molecules or siRNA results in mitotic defects resulting in cell death or senescence, supporting the promise for LSF inhibitory strategies as treatment for LSF-related cancers with high unmet medical needs.

bioRxiv preprint doi: https://doi.org/10.1101/665570; this version posted June 11, 2019. The copyright holder for this preprint (which was not certified by peer review) is the author/funder, who has granted bioRxiv a license to display the preprint in perpetuity. It is made available under aCC-BY 4.0 International license.

Introduction

LSF (encoded by *TFCP2*) is an evolutionarily conserved transcription factor that is normally expressed ubiquitously at low levels, but is significantly overexpressed in hepatocellular carcinoma cell lines and patient samples. Levels of LSF in patient samples from multiple populations rise with increased stage and severity of disease (1-4). Furthermore, LSF is oncogenic for hepatocellular carcinoma, as it is sufficient, in the background of a non-tumorigenic, but tumor-primed hepatocyte cell line, for hepatocellular carcinoma tumor growth in mouse xenograft models (1). Elevated LSF levels have also been documented in a number of other cancers, as well (5). In both colorectal cancer and hepatocellular carcinoma, patients with elevated LSF levels have significantly worse prognosis, with shorter median disease-free survival times than those with low LSF levels (3, 6). Finally, recent reports demonstrated that LSF can function as a co-activator for key transcription factors downstream of the Hippo and Wnt signaling pathways - YAP (4) and β-catenin (7) – both of which are widely accepted to contribute to liver proliferation and oncogenesis, as well as other cancer types.

Primary liver cancer and colorectal cancer are among the most common cancers worldwide (sixth and third, respectively), and represent leading causes of cancer mortality (second and fourth, respectively) (8-10). Although treatment options have improved, patients are often diagnosed with late stage, metastatic disease, resulting in high mortality. Hepatocellular carcinoma represents approximately 70-80% of primary liver cancer cases (9, 11). The only two FDA-approved therapies for late-stage hepatocellular carcinoma, Sorafenib and Regorafenib (multi-kinase inhibitors), unfortunately demonstrate only modest improvement in patient survival rates (12, 13), and result in significant side effects and rapid development of drug resistance. Thus, a large unmet medical need remains for hepatocellular carcinoma and colorectal patient populations. Therapies directed to distinct molecular targets, ideally to which the cancer is oncogene addicted, have been promoted for mitigating these diseases (11).

A family of small molecule inhibitors of LSF, Factor Quinolinone Inhibitors (FQIs), was identified that inhibits the DNA binding and transcription activity of LSF, but not that of transcription factors from multiple other structural classes (14). Activity of p53, the closest structural relative of the LSF family (15, 16), was also not inhibited by FQIs. Phenotypically, FQIs inhibit growth of hepatocellular carcinoma cells *in vitro*. They also inhibit hepatocellular

bioRxiv preprint doi: https://doi.org/10.1101/665570; this version posted June 11, 2019. The copyright holder for this preprint (which was not certified by peer review) is the author/funder, who has granted bioRxiv a license to display the preprint in perpetuity. It is made available under aCC-BY 4.0 International license.

carcinoma tumor growth *in vivo* in multiple mouse models, including a mouse endogenous liver tumor model (17). In all cases, inhibition of tumor growth occurred in the absence of toxicity, as assessed by liver injury markers, histopathology of tissues with rapid cell turnover, or blood cell counts (18). These results suggested that hepatocellular carcinoma cells are oncogene addicted to LSF (14, 19).

Oncogenic transcription factors are promising therapeutic targets given that they regulate tumorigenic pathways. However, transcription factors, in general, have been notoriously difficult to target with small molecule inhibitors as their DNA binding domains are commonly small and the proteins themselves are intrinsically disordered promiscuity (20). Identification of the transcription factor LSF as an oncogene and the significant inhibition of tumor growth upon LSF inhibition with no observed toxicity indicate that LSF holds considerable promise as a cancer therapeutic target (1, 14, 21). Targeting a transcription factor has been challenging, therefore validation of the biological specificity of the LSF inhibitors is essential. Here we demonstrate that the molecular and phenotypic consequences of knockdown of LSF with a specific siRNA are the same as treatment of cells with FQI1, therefore confirming that FQIs are highly specific in targeting this transcription factor.

The molecular mechanisms by which LSF promotes cancer cell survival has not been well characterized, although initial data indicated that FQIs induce a “prometaphase-like” arrest in hepatocellular carcinoma cells (17). Clarifying the pathways by which inhibition of LSF leads to cell death is important to further support the candidacy of FQIs as a molecular therapy. Cell cycle analysis by flow cytometry and time-lapse microscopy revealed mitotic defects including mitotic delays with condensed, but unaligned chromosomes, leading to increased time in mitosis, defective cell division, multi-nucleation, and apoptosis. In addition, loss of LSF activity induced senescence in a sub-population of cells in a dose-dependent manner. Senescence, as well as mitotic arrest and apoptosis, are all desirable outcomes for a cancer chemotherapeutic.

Materials and Methods

Preparation of FQI1

FQI1 was synthesized as previously described (14). FQI1 was dissolved in analytical grade DMSO (Sigma). The final DMSO concentration added to the cells was 0.5%.

bioRxiv preprint doi: https://doi.org/10.1101/665570; this version posted June 11, 2019. The copyright holder for this preprint (which was not certified by peer review) is the author/funder, who has granted bioRxiv a license to display the preprint in perpetuity. It is made available under aCC-BY 4.0 International license.

Cell lines and synchronization

HeLa cells (gift from Devanand Sarkar, Virginia Commonwealth University) were cultured at 37°C in 10 % CO_2 in DMEM (Corning Cellgro) supplemented with 10% Fetal Bovine Serum (FBS; Atlanta Biologicals). For synchronization using a double thymidine block protocol, cells were treated with 2 mM thymidine (Sigma) in complete medium for 18 hours, and then released into complete medium for 6 hours followed by incubation in 2 mM thymidine in complete medium for a second 18-hour incubation. For release from the G1/S block, cells were transferred into complete medium. The single thymidine block involved a single 24 hour incubation in 2 mM thymidine and release into complete media. As indicated, the release medium also contained 20 μM of thymidine.

siRNA transfection

siRNAs were designed and synthesized at Alnylam Pharmaceuticals, Inc. siRNA sequences used: LSF Sense: 5' GUGUGAUGUUUAAcAGGAATT 3'; LSF Antisense: 5' UUCCUGUUAAACAUCACACTT 3'; LBP1A Sense 5' UUUCAGGUGCCGACUUAUUTT 3'; LBP1A Antisense: 5' AAUAAGUCGGCACCUGAAATT 3'. The siRNAs were stabilized using certain chemical modifications as previously described allowing durable knockdown (22, 23). The siRNA control was a sequence targeting RNA encoding firefly luciferase and was, therefore, non-targeting in the cells utilized for these studies. Cells were transfected using RNAimax (Life Technologies) according to manufacturer's instructions. Transfection efficiency was measured by fluorescent microscopy 24 hours post transfection by cellular uptake of the Cy3 labeled control siRNA, and was determined to be >90%. For all siRNA experiments, the initial thymidine block was started 24 hours after transfection of the siRNA.

Time-lapse microscopy

In order to image cell cycle progression for HeLa cells, retroviral Packaging Cells (GP2-293; Clontech) were transfected with pVSV-G (Clontech) and a pBABE vector containing both a gene for YFP-tagged histone H2B protein and for a gene encoding G418 resistance (gift from Jagesh Shah laboratory, Harvard Medical School). The virus-containing supernatant was collected for transduction of HeLa cells and the population of resistant cells was selected with G418 (Gibco).

bioRxiv preprint doi: https://doi.org/10.1101/665570; this version posted June 11, 2019. The copyright holder for this preprint (which was not certified by peer review) is the author/funder, who has granted bioRxiv a license to display the preprint in perpetuity. It is made available under aCC-BY 4.0 International license.

For time-lapse microscopy of siRNA-treated cells, the HeLa cells expressing H2B-YFP were transfected and synchronized with a single thymidine block and release. After release, cells were imaged in CO_2 independent medium (Leibovitz's L-15 without phenol red) on a Nikon TA10 Eclipse with a 20X objective at 37°C. For time-lapse microscopy of FQI1-treated cells, HeLa cells expressing H2B-YFP were treated with either vehicle or 0.9, 1.8, or 3.6 µM FQI1 in CO_2 independent medium (Leibovitz's L-15 without phenol red). Cells were imaged immediately on a Nikon TA10 Eclipse with a 20X objective at 37°C. Images were acquired every four minutes at 7-10 positions per sample, over a five- to eleven-hour time span. Length of mitosis was measured from nuclear envelope breakdown to anaphase. Nuclear envelope breakdown was identified as the first image displaying disordered, condensed chromosomes. Anaphase was identified as the first image showing sister chromatid separation (for normal anaphases) or showing a furrow beginning to form over the chromosomes. For experiments, 100 to 101 cells were examined per condition.

Cell flow cytometry

Cells were harvested, washed, and fixed with ethanol. Cells were stained with the Guava cell cycle reagent (EMD Millipore) according to manufacturer's instructions. Fluorescence was analyzed on a BD Dickenson FACS Calibur.

Immunoblotting

Cells were lysed in RIPA buffer (125 mM Tris HCl, 150 mM NaCl, 0.1% NP-40, 1.0% Sodium deoxycholate, 1.0% SDS, pH 7.6) containing ROCHE protease cocktail phosphatase inhibitors (Sigma Aldrich 4693159001) at the manufacturer's recommended concentrations. Lysates were electrophoresed through 4-20% Mini-PROTEAN® TGX™ Precast gradient gels (Bio-rad). The proteins were transferred to a PVDF membrane, and membranes were incubated for 1 hour in odyssey blocking buffer (LI-COR Biosciences cat# 927-40000). Primary antibodies included Aurora Kinase B (Abcam AB2254), Cdc20 (Abcam AB26483), Cyclin B1 (AB72), LBP-1a (ABE181), LSF (Abcam ABE180), phosphorylated Histone 3 Serine 10 (Abcam ab5176), phosphorylated Histone 3 Serine 28 (Abcam, ab5169), and α-Tubulin (Sigma, 10002). Secondary antibodies were from LI-Cor, Inc. and included donkey anti-mouse IR800 (926-32212), donkey anti-rabbit IR800 (926-32213), goat anti-rabbit IR680 (926-68073), and goat anti-mouse IR680 (926-32214). PVDF membranes were imaged using the Licor Odyssey (24).

bioRxiv preprint doi: https://doi.org/10.1101/665570; this version posted June 11, 2019. The copyright holder for this preprint (which was not certified by peer review) is the author/funder, who has granted bioRxiv a license to display the preprint in perpetuity. It is made available under aCC-BY 4.0 International license.

Infrared detection quantitated each band on an individual pixel basis using western analysis tools in the Image Studio program.

Gene expression determination

For most experiments, RNA was isolated using the Qiagen RNAeasy kit following the manufacturer's instructions. cDNA was generated using a Reverse Transcription kit from Applied Biosystems (4368814). Probes for RNA quantification were acquired from Life Technologies with the Taqman gene expression system (Life Technologies). Target gene expression was normalized to a ubiquitous control (*GAPDH*) utilizing a dual label system. Cp values were measured using a Light Cycler 480 (Roche). The following probes were used: (*AURKB*) HS009645858 M1, (*CDC20*) HS00426680 M1, (*UBP1*, which encodes LBP1A) HS00232691 M1m, (*TFCP2*, which encodes LSF) HS00232185 M1, (*MAD2L1*) HS00365651 M1, and (*GAPDH*) 4333764F.

Cellular senescence measurement

HeLa cells were synchronized with a double thymidine block with either FQI1 treatment or LSF knockdown. The cells were stained for β-galactosidase using the activity kit (Kit 9860S) from Cell Signaling Technologies according to the manufacturer's protocol. Following the overnight incubation, cells were imaged on a phase Axiovert 40 CFL (Zeiss) microscope. The number of blue-staining cells was quantified, irrespective of the intensity of the signal, in comparison to the number of cells lacking blue staining.

Statistical analysis

Statistical significance was determined using a two-tailed Student T Test; *P<0.05, **P<0.01, ***P<0.001, ****P<0.0001.

Data Availability

The ChIP-seq data have been submitted to GEO. The data that support the findings of this study are available from the corresponding author upon request.

Results

Chemical inhibition of LSF induces mitotic defects

Previously, we reported that LSF inhibition by small molecule inhibitors (FQIs) resulted in cells delayed with G2/M ("4n") DNA content in hepatocellular carcinoma cell lines.

bioRxiv preprint doi: https://doi.org/10.1101/665570; this version posted June 11, 2019. The copyright holder for this preprint (which was not certified by peer review) is the author/funder, who has granted bioRxiv a license to display the preprint in perpetuity. It is made available under aCC-BY 4.0 International license.

Furthermore, fluorescent staining of synchronized cells for DNA and tubulin demonstrated that when control cells completed mitosis and re-entered G1, FQI-treated cells generally remained in mitosis with condensed but unaligned DNA (17). In order to elucidate the basis for these FQI1-mediated mitotic defects and their consequences in greater detail, and over a range of FQI1 concentrations, we synchronized HeLa cells, which demonstrate the same phenotype, with a double thymidine block (Fig. 1A), and analyzed samples for cellular DNA content throughout the subsequent cell cycle. At 1.8 µM, FQI1-treated cells were initially delayed in returning from G2/M to G1, remaining with 4n DNA content, compared to control cells that had re-entered G1 (Fig. 1B, 8.5 h), an observation consistent with previous studies (17). Following this delay, a mix of phenotypic outcomes was observed at 20 hours after release from G1/S, with FQI1-treated cells having divided to a 2n DNA content, initiated cell death pathways (subG1 DNA content), or retained their duplicated DNA content. At the highest FQI1 concentration tested (3.6 µM), cells were also initially delayed with 4n DNA content, but a large fraction of the population converted to subG1 DNA content by 20 hours post release from the G1/S block (Fig. 1B).

Given limitations in interpretation of population-wide data, it was critical to analyze the phenotype(s) on a per cell basis upon inhibition of LSF. Using HeLa cells stably expressing fluorescently labeled histone H2B chromosomal DNA was visualized as cells passed through mitosis by time-lapse microscopy. Asynchronous H2B-YFP-expressing cells were treated with increasing concentrations of FQI1. At 1.8 µM (Fig. 1C) mitotic progression was delayed with condensed, unaligned chromosomes. Cells subsequently appeared to exit mitosis without proper chromosome segregation, resulting in a multinuclear (4n) G1 state (Fig. 1C) (17). In contrast, cells treated with vehicle progressed through mitosis normally (Fig. 1C and D). Mitotic time (time from nuclear envelope breakdown (NEB) to anaphase) was dose-dependent, increasing with increasing concentrations of FQI1 (Fig. 1D). At the lower concentrations of FQI1, cells exited mitosis aberrantly after the mitotic delay (Fig. 1C, D and E). However for cells treated with 3.6 µM FQI1, mitotic time was indeterminable (Fig. 1E); cells arrested with condensed but unaligned chromosomes but never exited mitosis, either normally or aberrantly, throughout the 640 minutes of imaging (Supplementary Fig. S1A).

In some cell lines, LSF is necessary for upregulation of thymidylate synthase expression and therefore efficient transition through S phase (25). However, our previous studies indicated that

bioRxiv preprint doi: https://doi.org/10.1101/665570; this version posted June 11, 2019. The copyright holder for this preprint (which was not certified by peer review) is the author/funder, who has granted bioRxiv a license to display the preprint in perpetuity. It is made available under aCC-BY 4.0 International license.

adequate thymidylate synthase expression is achieved despite reduction in LSF activity (14, 26). Nonetheless, since S phase defects can ultimately lead to mitotic defects, DNA damage was monitored by measuring phosphorylated H2AX (γ-H2AX) chromosomal foci. Cells treated with 1.8 μM FQI1 or vehicle during synchronization were analyzed for γ-H2AX by immunofluorescence 8 hours after release from the G1/S block (Fig. 1F). UV-irradiated cells, a positive control, demonstrated extensive γ-H2AX staining. In contrast, only comparable, low levels of phosphorylated H2AX were visualized in both the vehicle- and FQI1-treated cells, consistent with low levels of DNA damage known to occur in cancer cells (27). These data suggest that FQI1-mediated mitotic defects are due to a direct requirement for LSF in regulating proper progression through mitosis.

LSF small molecule inhibition during cell synchronization results in reduced expression of key mitotic regulators

Upon LSF activity inhibition, we observed defects in chromosome alignment and segregation, resulting in mitotic delay and multi-nucleation: phenotypes previously reported following inhibition or deficiency of major mitotic regulators Aurora kinase B (*AURKB*) and Cyclin Division Cycle 20 (*CDC20*) (28, 29). To investigate whether inhibition of LSF alters expression of *AURKB* and *CDC20* RNA, HeLa cells were synchronized with a double thymidine block (Fig. 2A). RNA levels were measured in vehicle-treated cells at the G1/S border (0 hours) and as cells progressed to or just through mitosis (8 hours), as demonstrated by DNA profiling (Fig. 1B) and fluorescence microscopy (Supplementary Fig. S1B). As expected, mitotic expression of *CDC20* was elevated approximately 6-fold compared to RNA levels at G1/S (Supplementary Fig. S1C). However, *AURKB* RNA levels in vehicle-treated cells increased only 1.2 fold in mitosis, consistent with dysregulated overexpression in these cancer cells. Incubation with 1.8 μM FQI1 during the synchronization protocol resulted in reduction of both *AURKB* and *CDC20* RNA levels compared to the control cells 8 hours post release (Fig. 2B). Consistent with transcript reduction, AURKB and CDC20 protein levels were also reduced in a dose-dependent manner (Fig. 2C and 2D), whereas LSF protein levels were unchanged, as expected (Fig. 2C). The impact of the downregulation of AURKB was tested by monitoring phosphorylation of an AURKB substrate. Phosphorylation of Histone 3 on Serine 10 (30) was reduced by FQI1 in a dose-dependent manner (Fig. 2C and 2D).

bioRxiv preprint doi: https://doi.org/10.1101/665570; this version posted June 11, 2019. The copyright holder for this preprint (which was not certified by peer review) is the author/funder, who has granted bioRxiv a license to display the preprint in perpetuity. It is made available under aCC-BY 4.0 International license.

The mitotic phenotypes would indeed be consistent with inhibition of Aurora kinase B and/or CDC20. Aurora kinase B inhibition leads to defects in kinetochore-microtubule attachment and cytokinesis, followed by multinucleation (31, 32), and knockdown of CDC20 results in an increase in mitotic time (29). In addition, both LSF and AURKB are upregulated in hepatocellular carcinoma patient samples, with each positively correlating with disease severity (1, 33). However, in contrast to previous results in asynchronous cells (17), Cyclin B levels were also downregulated (Fig. 2C), particularly when cells were treated with the highest concentrations of FQI1 during the synchronization procedure. This finding suggested that cells treated with FQI1 during synchronization are not efficiently proceeding through the cell cycle into mitosis after the G1/S arrest, complicating straightforward interpretation of the gene expression results. Due to the induction of cell cycle defects upon LSF inhibition, the protein expression data could not therefore distinguish whether downregulation of AURKB and CDC20 was the cause or consequence of the phenotypic outcomes.

In order to distinguish whether diminished *AURKB* and *CDC20* gene expression resulted from lack of cell cycle progression of LSF inhibited cells or from diminished expression of these genes in mitosis, we analyzed RNA in synchronized, LSF-inhibited cells only from cells in mitosis, isolated by the standard mitotic shakeoff methodology (Supplementary Fig. S2A-B). A reproducible decrease in *CDC20*, but not *AURKB*, RNA was observed. As an alternative method to identify candidate LSF target genes, we sought to identify genes around which LSF binds. The absence of a sufficiently robust antibody against LSF for chromatin immunoprecipitation (ChIP) prevented testing for endogenous LSF. Instead, a HEK cell line expressing an inducible, HA-tagged LSF (14) was used for initial ChIP-sequencing analysis. Multiple HA-LSF binding peaks were observed around the *AURKB* gene (Supplementary Fig. S2C), and binding of LSF was validated both at the *AURKB* promoter and around 3000 bp upstream of the transcription start site by quantitative PCR (Supplementary Fig. S2D). In contrast, no HA-LSF binding peaks were observed within 20 kb of the *CDC20* gene. Taken in combination, whether LSF activates *AURKB* expression in these, or other, cells remains unresolved. However, these data suggest that LSF may regulate *CDC20* expression, although either indirectly or from distant binding sites. Global gene expression data from cells treated with FQI1 between G1/S and mitosis did not

bioRxiv preprint doi: https://doi.org/10.1101/665570; this version posted June 11, 2019. The copyright holder for this preprint (which was not certified by peer review) is the author/funder, who has granted bioRxiv a license to display the preprint in perpetuity. It is made available under aCC-BY 4.0 International license.

identify dysregulation of any other mitotic regulators that would cause an early mitotic delay (34).

RNAi mediated knockdown of LSF phenocopies inhibition of LSF with the small molecule inhibitor FQI1

A critical aspect of interpreting the data with FQI1 was to determine whether its effects truly reflected inhibition of the identified target. FQI1 inhibits LSF DNA-binding and protein-binding activities, whereas it does not impact activity of a number of other transcription factors, both of disparate and similar structural domains (14, 35). These data support that targeting of LSF by FQIs is highly specific. Furthermore, since only LSF, but not its other widely-expressed paralog, LBP1A, is overexpressed in hepatocellular carcinoma or as yet implicated in cancer (1, 5), we predicted that knockdown of LSF alone would cause the same molecular and phenotypic outcomes in these cells as those caused by FQI1. Although LSF has a half-life of approximately 24 hours (36), we identified an siRNA that resulted in robust and durable knockdown of LSF (Fig. 3B and C, Supplementary Fig. S3A-C). In addition, since certain siRNAs can cause nonspecific reduction in mRNA encoding MAD2 (37), which controls the spindle assembly checkpoint, we verified that the selected siRNA targeting LSF did not inadvertently reduce *MAD2L1* transcript levels (Supplementary Fig. S3D).

In order to compare downstream molecular outcomes from FQI1 and LSF siRNA treatments, whether direct or indirect, *AURKB* or *CDC20* RNA levels were measured following RNAi mediated knockdown of either LSF or a non-expressed control. HeLa cells were transfected with siRNAs, to initiate protein knockdown, 30 hours prior to synchronization. RNA and protein expression were analyzed at two time points - when control cells were arrested at G1/S (0 hours) and when these cells were largely in mitosis after release from the block (8 hours) (Fig. 3A, Supplementary Fig. S4A). For ease of comparison, RNA levels were plotted relative to the level in the control siRNA sample at each time point. At 20 nM siRNA, significant knockdown of both LSF-encoding RNA (Fig. 3B) and protein (Fig. 3C) were achieved over this time course. Consistent with the results generated with the LSF small molecule inhibitor at 8 hours after G1/S release (Fig. 2B), *AURKB* and *CDC20* RNA levels were reduced (Fig. 3B). Immunoblotting of lysates harvested at the approximate time of mitotic entry of the control cells (8 hours) confirmed a dose-dependent reduction in AURKB and CDC20 protein levels after

bioRxiv preprint doi: https://doi.org/10.1101/665570; this version posted June 11, 2019. The copyright holder for this preprint (which was not certified by peer review) is the author/funder, who has granted bioRxiv a license to display the preprint in perpetuity. It is made available under aCC-BY 4.0 International license.

siRNA-mediated knockdown of LSF (Fig. 3C and D), consistent with the findings upon inhibition of LSF with FQI1 (Fig. 2C). As expected, phosphorylation of AURKB substrates Serine 10 and 28 of histone H3 (30, 38) was reduced. As with FQI1 treatments, Cyclin B levels were also reduced in a dose-dependent manner. Thus, LSF siRNA phenocopied the molecular consequences of FQI1 on gene expression, whether due to direct transcriptional effects, and/or consequences of cell cycle dysregulation.

To determine whether LSF knockdown resulted in similar cellular phenotypes to those observed with FQI1, synchronized YFP-H2B-expressing HeLa cells were transfected with siRNAs targeting LSF or a non-expressed control. A single thymidine block protocol was sufficient for synchronization (Fig. 4A), as mitotic progression is viewed on a cell-by-cell basis. Representative time-lapse images of cells treated with the highest concentration (20 nM) of either LSF targeting siRNA or control siRNA highlight dramatic changes in mitotic progression. Control cells exhibited progression through normal mitotic phases in a timely manner (Fig. 4B). However, cells with diminished LSF levels exhibited an extensive delay with condensed, but unaligned chromosomes, generally followed by defective cellular division and multinucleation (Fig. 4B). In addition, some cells remained in mitosis with condensed chromosomes throughout the entire time lapse analysis. Upon quantitation mitotic time was dramatically increased when LSF levels were reduced (Fig. 4C). Counterintuitively, the lower concentrations of LSF siRNA resulted in longer times for mitotic progression. We propose that at the higher LSF knockdown conditions the more defective cells are unlikely to enter mitosis, thus selecting for a less severe population available for the analysis. Indeed, when siRNA-transfected cells were imaged by time lapse microscopy after a double thymidine block, there was an inverse correlation between higher levels of LSF knockdown and the number of cells capable of entering mitosis (Supplementary Fig. S4B).

By histone H2B fluorescence, the most striking mitotic outcome for individual cells treated with LSF siRNA after the extended delay in mitosis appeared to be mitotic slippage (Fig. 4B). This was confirmed by immunofluorescence of synchronized cell populations, co-stained for DNA and α-tubulin (Supplementary Fig. S5A-B). Quantitation of these immunofluorescence data demonstrated significant increases in cells with condensed, but nonaligned chromosomes, incomplete cytokinesis, and multinucleation upon LSF knockdown. These phenotypes mimicked

bioRxiv preprint doi: https://doi.org/10.1101/665570; this version posted June 11, 2019. The copyright holder for this preprint (which was not certified by peer review) is the author/funder, who has granted bioRxiv a license to display the preprint in perpetuity. It is made available under aCC-BY 4.0 International license.

those observed with FQI1 treatment (Supplementary Fig. S5C-D). Finally, both types of treatments yielded mitotic cells with cellular protrusions (Supplementary Fig. S5E).

Also consistent with the results from FQI1 treatment, knockdown of LSF did not induce phosphorylated H2AX (γ-H2AX) foci, as monitored the beginning of mitosis in a synchronized cell population (Fig. 4E). This result suggests that the effects of inhibiting LSF on mitotic progression are not due to defects induced indirectly in S phase.

Since FQI1 also inhibits activity of paralog LBP1A (T. Grant, unpublished observations), a widely expressed paralog of LSF (39), we also investigated the mitotic phenotypes upon LBP1A siRNA treatment. The identified siRNA resulted in robust and durable knockdown of LBP1A (Supplementary Fig. S6A-B), with no reduction in *MAD2L1* transcript levels (Supplementary Fig. S6C). Knockdown of LBP1A did reduce overall cell proliferation to some extent, but much less so than did knockdown of LSF (Supplementary Fig. S7A). Despite that proliferative effect, LBP1A knockdown did not significantly diminish cell viability, in stark contrast to consequences of LSF knockdown and FQI1 treatment (Supplementary Fig. S7B-C). Furthermore, LBP1A knockdown did not observably inhibit mitotic progression as measured by cellular DNA profiling (Supplementary Fig. S7D). However, time-lapse microscopy did detect a subtle (1.5–fold) increase in mitotic time upon LBP1A knockdown alone (Supplementary Fig. S7E), consistent with the diminished cell proliferation. No abnormal mitotic phenotypes were observed either by time-lapse or immunofluorescent microscopy. Given the minimal consequences upon inhibiting LBP1A, we conclude that inhibition of LSF activity is what drives the dramatic FQI1-mediated mitotic defects.

Induction of cellular senescence following inhibition of LSF

In addition to mitotic delay resulting from LSF inhibition, some cells undergoing synchronization while inhibiting LSF were arrested at other points in the cell cycle:cellular DNA profiling of FQI1- or LSF siRNA-treated cells being synchronized with a double thymidine block, captured cells that no longer progressed from the 2n state into S phase upon release from the G1/S block (Fig. 1B, Supplementary Fig. S4A), and time-lapse microscopy showed that a considerable fraction of the cells treated with LSF siRNA during a double thymidine block never entered mitosis during 10-12 hours after release from the G1/S block (Supplementary Fig. S4B). Mitotic defects, caused by multiple distinct insults, can lead to senescence after G1 re-entry with

bioRxiv preprint doi: https://doi.org/10.1101/665570; this version posted June 11, 2019. The copyright holder for this preprint (which was not certified by peer review) is the author/funder, who has granted bioRxiv a license to display the preprint in perpetuity. It is made available under aCC-BY 4.0 International license.

either 2n or 4n DNA content (40, 41). Thus, we hypothesized that mitotic defects from decreasing LSF levels or activity during previous cell divisions resulted in senescence. To test this hypothesis, HeLa cells were synchronized as before by a double thymidine block in the presence of FQI1, or LSF siRNA, and analyzed for senescence by monitoring β-galactosidase activity at low pH (42) at a time point when control cells entered mitosis. Both reduction in LSF levels and inhibition of LSF activity resulted in significantly greater numbers of β-galactosidase-positive cells (stained blue) compared to the respective controls (Fig. 5A-B). Overall, there was a 3- to 5-fold increase in senescent cells with increasing amounts of LSF inhibition, although treatment with 0.9 μM FQI1 was not sufficient to induce senescence. These data show that inhibition of LSF can result in senescence of cancer cells, and support the hypothesis that reduced LSF levels or activity during previous cell cycle(s) can predispose cells to senescence.

Discussion

The transcription factor LSF is an oncogene in multiple cancer types, notably including hepatocellular carcinoma (1, 5, 21). Small molecule inhibitors directly targeting LSF inhibited hepatocellular carcinoma cell proliferation i*n vitro* and tumor growth *in vivo* with no signs of toxicity at doses required for tumor inhibition (14, 17, 18). Together, these data indicate that LSF is a promising therapeutic candidate for hepatocellular carcinoma patients, and likely for other cancer types. The robust anti-tumor activity of FQIs is consistent with the initial report that a dominant negative LSF reduced tumorigenicity (1). Given the difficulties generally encountered in targeting transcription factors with small molecules (20), further investigation was warranted to confirm that anti-tumor effects of FQIs were due to specific targeting of LSF. Here, we demonstrated that a siRNA targeting LSF produced strikingly similar results to that of FQI1 treatment in all aspects, confirming specific targeting by the small molecule inhibitor. Furthermore, knockdown of the close LSF paralog, LBP1A, did not result in such mitotic defects. Thus, we conclude that LSF is the factor required for accurate and efficient mitotic progression in these cancer cells.

The simplest interpretation from the mitotic phenotypes observed is that, as a transcription factor, LSF directly regulates expression of mitotic regulators. Indeed, both FQI1 and LSF siRNA result in downregulation of *AURKB* and *CDC20* expression. However, further

bioRxiv preprint doi: https://doi.org/10.1101/665570; this version posted June 11, 2019. The copyright holder for this preprint (which was not certified by peer review) is the author/funder, who has granted bioRxiv a license to display the preprint in perpetuity. It is made available under aCC-BY 4.0 International license.

examination indicates that these consequences may be indirect. Furthermore, it is noteworthy that unlike the emphasis on Cyclin B levels in a previous report (17) in which asynchronous cells were treated with FQI1, when synchronized cells were examined Cyclin B protein levels in 1.8 µM FQI1-treated cells were similar to those in control cells, and certainly not increased (Fig. 2C). We conclude that the increase in cyclin B protein levels observed in Rajasekaran et al. resulted simply from accumulation of cells in mitosis when treated with 2 µM for 12-24 hours, whereas the control cells were continually cycling in those asynchronous populations. This underscores the need to perform experiments in synchronized cells, as was done here. Further investigations in synchronized cell populations are ongoing to demonstrate the mechanistic basis for the profound mitotic defects leading to apoptosis or senescence that result from LSF inhibition.

It has been previously demonstrated that LSF inhibition limits tumor progression, and that LSF inhibition causes apoptosis in multiple hepatocellular carcinoma cell lines (14, 17), as demonstrated here by HeLa cells with sub-G1 cellular DNA content (Fig. 1A, Supplementary Fig. S4). Here, we report for the first time that senescence can also be induced by LSF inhibition in cancer cells. Using both small molecule inhibition and siRNA knockdown, the percentage of senescent cells was proportional to the extent of inhibition of LSF during the synchronization protocol (Fig. 5). Both senescence and apoptosis are desirable outcomes for treatment of cancer.

Since both small molecule inhibitors and siRNAs targeting LSF can lead to cancer cell death or senescence *in vitro*, it is worthwhile to consider the targeting strategy for LSF inhibition in patients. Many cancer drug candidates target mitosis in an effort to exploit this key vulnerability of cancer cells. However, many such therapies have failed in trials, which may result from: (1) tumor escape, where pathway redundancy or evasive resistance in mammalian cells enables the tumor cell to escape the therapy (43, 44), or (2) low mitotic index where the drug half-life may not be long enough to suppress the target when cell division is triggered for any particular tumor cell (45, 46). As a target, LSF may have an advantage toward avoiding tumor escape. Inhibiting a transcription factor can target multiple pathways simultaneously, thus the likelihood that system redundancy would fully compensate is diminished. In addition, the issue of low mitotic index may be avoidable for the LSF inhibitors, since the apparent lack of toxicity in preclinical models may permit dosing in manners that generate sustained drug levels. Gene

bioRxiv preprint doi: https://doi.org/10.1101/665570; this version posted June 11, 2019. The copyright holder for this preprint (which was not certified by peer review) is the author/funder, who has granted bioRxiv a license to display the preprint in perpetuity. It is made available under aCC-BY 4.0 International license.

silencing based approaches may also provide a useful strategy to counter low mitotic index for hepatocellular carcinoma patients. The first RNAi drug, which uses a lipid nanoparticle to encapsulate and efficiently deliver siRNA to hepatocytes, was recently approved following robust and durable gene silencing over the 18-month pivotal study (47). Additionally, a ligand-based strategy to deliver LSF siRNA to hepatocytes may provide added benefit as recent human data using a triantennary *N*-acetylgalactosamine (GalNAc) mediated siRNA delivery system demonstrated robust knockdown of a hepatic target that was sustained for more than a year (48, 49). The target of GalNAc, asialoglycoprotein receptor (ASGR1) (23), is expressed , in early stages and often in later stages of hepatocellular carcinoma (50), although whether tumors retain ubiquitous expression is not clear.

In summary, comparing cellular and molecular outcomes of small molecule inhibitors that eliminate LSF activity to those of RNAi that specifically targets LSF, the specificity of FQI1 for LSF was confirmed. Both mechanisms resulted in similar mitotic defects, followed by cellular death or senescence, proving that LSF regulates mitosis in cancer cells. Therefore, the anti-tumor activity of FQI1 in multiple preclinical models is explicitly due to loss of LSF activity. These findings support the candidacy of LSF targeting agents for treatment of hepatocellular carcinoma and other cancers in which LSF is identified as an oncogene.

bioRxiv preprint doi: https://doi.org/10.1101/665570; this version posted June 11, 2019. The copyright holder for this preprint (which was not certified by peer review) is the author/funder, who has granted bioRxiv a license to display the preprint in perpetuity. It is made available under aCC-BY 4.0 International license.

References

1. Yoo BK, Emdad L, Gredler R, Fuller C, Dumur CI, Jones KH, et al. Transcription factor Late SV40 Factor (LSF) functions as an oncogene in hepatocellular carcinoma. Proc Natl Acad Sci U S A 2010;107:8357-62.

2. Fan R-H, Li J, Wu N, Chen P-S. Late SV40 factor: A key mediator of Notch signaling in human hepatocarcinogenesis. World J Gastroenterol 2011;17:3420-30.

3. Kim JS, Son SH, Kim MY, Choi D, Jang I-S, Paik SS, et al. Diagnostic and prognostic relevance of CP2c and YY1 expression in hepatocellular carcinoma. Oncotarget 2017;8:24389-400.

4. Zhang X, Sun F, Qiao Y, Zheng W, Liu Y, Chen Y, et al. TFCP2 Is Required for YAP-Dependent Transcription to Stimulate Liver Malignancy. Cell Rep 2017;21:1227-39.

5. Kotarba G, Krzywinska E, Grabowska AI, Taracha A, Wilanowski T. TFCP2/TFCP2L1/UBP1 transcription factors in cancer. Cancer Lett 2018;420:72-9.

6. Jiang H, Du J, Jin J, Qi X, Pu Y, Fei B. LSF expression and its prognostic implication in colorectal cancer. Int J Clin Exp Pathol 2014;7:6024-31.

7. Yuedi D, Yuankun C, Jiaying Z, Han L, Yueqi W, Houbao L, et al. TFCP2 activates beta-catenin/TCF signaling in the progression of pancreatic cancer. Oncotarget 2017;8:70538-49.

8. Laursen L. A preventable cancer. Nature 2014;516:S2-S3.

9. Llovet JM, Villanueva A, Lachenmayer A, Finn RS. Advances in targeted therapies for hepatocellular carcinoma in the genomic era. Nat Rev Clin Oncol 2015;12:408-24.

10. Torre LA, Bray F, Siegel RL, Ferlay J, Lortet-Tieulent J, Jemal A. Global cancer statistics, 2012. CA Cancer J Clin 2015;65:87-108.

11. Torrecilla S, Llovet JM. New molecular therapies for hepatocellular carcinoma. Clin Res Hepatol Gastroenterol 2015;39:S80-S85.

12. Llovet JM, Ricci S, Mazzaferro V, Hilgard P, Gane E, Blanc J-F, et al. Sorafenib in advanced hepatocellular carcinoma. N Engl J Med 2008;359:378-90.

13. Bruix J, Qin S, Merle P, Granito A, Huang Y-H, Bodoky G, et al. Regorafenib for patients with hepatocellular carcinoma who progressed on sorafenib treatment (RESORCE): a randomised, double-blind, placebo-controlled, phase 3 trial. Lancet 2017;389:56-66.

bioRxiv preprint doi: https://doi.org/10.1101/665570; this version posted June 11, 2019. The copyright holder for this preprint (which was not certified by peer review) is the author/funder, who has granted bioRxiv a license to display the preprint in perpetuity. It is made available under aCC-BY 4.0 International license.

14. Grant TJ, Bishop JA, Christadore LM, Barot G, Chin HG, Woodson S, et al. Antiproliferative small molecule inhibitors of transcription factor LSF reveal oncogene addiction to LSF in hepatocellular carcinoma. Proc Natl Acad Sci USA 2012;109:4503-8.

15. Kokoszynska K, Ostrowski J, Rychlewski L, Wyrwicz LS. The fold recognition of CP2 transcription factors gives new insights into the function and evolution of tumor suppressor protein p53. Cell Cycle 2008;7:2907-15.

16. Ming Q, Roske Y, Schuetz A, Walentin K, Ibraimi I, Schmidt-Ott KM, et al. Structural basis of gene regulation by the Grainyhead/CP2 transcription factor family. Nucleic Acids Res 2018;46:2082-95.

17. Rajasekaran D, Siddiq A, Willoughby JLS, Biagi JM, Christadore LM, Yunes SA, et al. Small molecule inhibitors of Late SV40 Factor (LSF) abrogate hepatocellular carcinoma (HCC): Evaluation using an endogenous HCC model. Oncotarget 2015;6:26266-77.

18. Willoughby JLS. Transcription factor LSF: A mitotic regulator in hepatocellular carcinoma Boston University; 2016.

19. Shlomai A. Targeting late SV40 factor: Is the achilles heel of hepatocarcinogenesis revealed? World J Gastroenterol 2012;18:6709-11.

20. Dunker AK, Uversky VN. Drugs for 'protein clouds': targeting intrinsically disordered transcription factors. Curr Opin Pharmacol 2010;10:782-8.

21. Santhekadur PK, Rajasekaran D, Siddiq A, Gredler R, Chen D, Schaus SE, et al. The transcription factor LSF: a novel oncogene for hepatocellular carcinoma. Am J Cancer Res 2012;2:269-85.

22. Akinc A, Goldberg M, Qin J, Dorkin JR, Gamba-Vitalo C, Maier M, et al. Development of lipidoid-siRNA formulations for systemic delivery to the liver. Mol Ther 2009;17:872-9.

23. Nair JK, Willoughby JLS, Chan A, Charisse K, Alam MR, Wang Q, et al. Multivalent N-acetylgalactosamine-conjugated siRNA localizes in hepatocytes and elicits robust RNAi-mediated gene silencing. J Am Chem Soc 2014;136:16958-61.

24. Boveia V, Schutz-Geschwender A. Quantitative Analysis of Signal Transduction with In-Cell Western Immunofluorescence Assays. Methods Mol Biol 2015;1314:115-30.

25. Powell CMH, Rudge TL, Zhu Q, Johnson LF, Hansen U. Inhibition of the mammalian transcription factor LSF induces S-phase-dependent apoptosis by downregulating thymidylate synthase expression. EMBO J 2000;19:4665-75.

26. Yoo BK, Gredler R, Vozhilla N, Su Z, Chen D, Forcier T, et al. Identification of genes conferring resistance to 5-fluorouracil. Proc Natl Acad Sci U S A 2009;106:12938-43.

bioRxiv preprint doi: https://doi.org/10.1101/665570; this version posted June 11, 2019. The copyright holder for this preprint (which was not certified by peer review) is the author/funder, who has granted bioRxiv a license to display the preprint in perpetuity. It is made available under aCC-BY 4.0 International license.

27. Ji J, Zhang Y, Redon CE, Reinhold WC, Chen AP, Fogli LK, et al. Phosphorylated fraction of H2AX as a measurement for DNA damage in cancer cells and potential applications of a novel assay. PLoS ONE 2017;12:e0171582.

28. Girdler F, Gascoigne KE, Eyers PA, Hartmuth S, Crafter C, Foote KM, et al. Validating Aurora B as an anti-cancer drug target. J Cell Sci 2006;119:3664-75.

29. Huang H-C, Shi J, Orth JD, Mitchison TJ. Evidence that mitotic exit is a better cancer therapeutic target than spindle assembly. Cancer Cell 2009;16:347-58.

30. Crosio C, Fimia GM, Loury R, Kimura M, Okano Y, Zhou H, et al. Mitotic phosphorylation of histone H3: spatio-temporal regulation by mammalian Aurora kinases. Mol Cell Biol 2002;22:874-85.

31. Kitzen JJEM, de Jonge MJA, Verweij J. Aurora kinase inhibitors. Crit Rev Oncol Hematol 2010;73:99-110.

32. Nair JS, Ho AL, Tse AN, Coward J, Cheema H, Ambrosini G, et al. Aurora B kinase regulates the postmitotic endoreduplication checkpoint via phosphorylation of the retinoblastoma protein at serine 780. Mol Biol Cell 2009;20:2218-28.

33. Lin Z-Z, Jeng Y-M, Hu F-C, Pan H-W, Tsao H-W, Lai P-L, et al. Significance of *Aurora B* overexpression in hepatocellular carcinoma. *Aurora B* overexpression in HCC. BMC Cancer 2010;10:461.

34. Christadore LM. Discovery of a small molecule dihydroquinolinone inhibitor with potent antiproliferative and antitumor activity results in catastrophic cell division Boston University; 2013.

35. Chin HG, Ponnaluri VKC, Zhang G, Estève P-O, Schaus SE, Hansen U, et al. Transcription factor LSF-DNMT1 complex dissociation by FQI1 leads to aberrant DNA methylation and gene expression. Oncotarget 2016;7:83627-40.

36. Hansen U, Owens L, Saxena UH. Transcription factors LSF and E2Fs: Tandem cyclists driving G0 to S? Cell Cycle 2009;8:2146-51.

37. Hübner NC, Wang LHC, Kaulich M, Descombes P, Poser I, Nigg EA. Re-examination of siRNA specificity questions role of PICH and Tao1 in the spindle checkpoint and identifies Mad2 as a sensitive target for small RNAs. Chromosoma 2010;119:149-65.

38. Goto H, Yasui Y, Nigg EA, Inagaki M. Aurora-B phosphorylates Histone H3 at serine28 with regard to the mitotic chromosome condensation. Genes Cells 2002;7:11-7.

39. Ramamurthy L, Barbour V, Tuckfield A, Clouston DR, Topham D, Cunningham JM, et al. Targeted disruption of the CP2 gene, a member of the NTF family of transcription factors. J Biol Chem 2001;276:7836-42.

bioRxiv preprint doi: https://doi.org/10.1101/665570; this version posted June 11, 2019. The copyright holder for this preprint (which was not certified by peer review) is the author/funder, who has granted bioRxiv a license to display the preprint in perpetuity. It is made available under aCC-BY 4.0 International license.

40. Sadaie M, Dillon C, Narita M, Young ARJ, Cairney CJ, Godwin LS, et al. Cell-based screen for altered nuclear phenotypes reveals senescence progression in polyploid cells after Aurora kinase B inhibition. Mol Biol Cell 2015;26:2971-85.

41. Nakayama Y, Inoue T. Antiproliferative Fate of the Tetraploid Formed after Mitotic Slippage and Its Promotion; A Novel Target for Cancer Therapy Based on Microtubule Poisons. Molecules 2016;21:663.

42. Debacq-Chainiaux F, Erusalimsky JD, Campisi J, Toussaint O. Protocols to detect senescence-associated beta-galactosidase (SA-βgal) activity, a biomarker of senescent cells in culture and *in vivo*. Nat Protoc 2009;4:1798-806.

43. Bergers G, Hanahan D. Modes of resistance to anti-angiogenic therapy. Nat Rev Cancer 2008;8:592-603.

44. von Manstein V, Yang CM, Richter D, Delis N, Vafaizadeh V, Groner B. Resistance of Cancer Cells to Targeted Therapies Through the Activation of Compensating Signaling Loops. Curr Signal Transduct Ther 2013;8:193-202.

45. Chan K-S, Koh C-G, Li H-Y. Mitosis-targeted anti-cancer therapies: where they stand. Cell Death Dis 2012;3:e411.

46. Otto T, Sicinski P. Cell cycle proteins as promising targets in cancer therapy. Nat Rev Cancer 2017;17:93-115.

47. Adams D, Gonzalez-Duarte A, O'Riordan WD, Yang C-C, Ueda M, Kristen AV, et al. Patisiran, an RNAi Therapeutic, for Hereditary Transthyretin Amyloidosis. N Engl J Med 2018;379:11-21.

48. Pasi KJ, Rangarajan S, Georgiev P, Mant T, Creagh MD, Lissitchkov T, et al. Targeting of Antithrombin in Hemophilia A or B with RNAi Therapy. N Engl J Med 2017;377:819-28.

49. Huang Y. Preclinical and Clinical Advances of GalNAc-Decorated Nucleic Acid Therapeutics. Mol Ther Nucleic Acids 2017;6:116-32.

50. Shi B, Abrams M, Sepp-Lorenzino L. Expression of asialoglycoprotein receptor 1 in human hepatocellular carcinoma. J Histochem Cytochem 2013;61:901-9.

bioRxiv preprint doi: https://doi.org/10.1101/665570; this version posted June 11, 2019. The copyright holder for this preprint (which was not certified by peer review) is the author/funder, who has granted bioRxiv a license to display the preprint in perpetuity. It is made available under aCC-BY 4.0 International license.

Figure Legends

Figure 1. FQI1-treated HeLa cells exhibit mitotic defects. **A.** Schematic of experimental protocol. FQI1 or vehicle was added to HeLa cells during synchronization to the G1/S border using a double thymidine block. Cells released from the block in the presence of the FQI1 or vehicle, plus 20 µM of thymidine, were harvested at multiple times during progression through the cell cycle. **B.** At the indicated time points following release from the G1/S block with 0, 0.9, 1.8, or 3.6 µM of FQI1, cells were analyzed for DNA profiling by flow cytometry. Data are representative of at least three independent experiments. **C.** Representative time-lapse images of individual cells treated with vehicle or 1.8 µM FQI1. Numbers represent the time (in minutes) for one particular cell in the image from nuclear envelope breakdown (designated as time=0 for that cell). **D.** Quantitation of mitotic time from nuclear envelop breakdown (NEB) to anaphase for the population of asynchronous cells during treatment for approximately 16 hours with FQI1 or vehicle. Mitotic times (mean time in minutes +/- standard error of the mean, n) for vehicle, and 0.9 or 1.8 µM FQI1 treatments were: 48.7 +/- 1.5, 104; 84.5 +/- 4.9, 104; and 228 +/- 15, 77; respectively. Mitotic time for cells treated with 3.6 µM was not quantifiable, as those cells that entered mitosis during the imaging period never reached anaphase or nuclear division.
E. Quantitation of cellular events at increasing concentrations of FQI1 during the time lapse microscopy, including percentage of cells that entered mitosis but were delayed with condensed, but unaligned chromosomes, and the percentage that apparently underwent mitotic slippage with formation of multiple (>2) nuclei. 120-140 cells were analyzed for each concentration of FQI1, including vehicle alone. **F.** Bottom: γ-H2AX staining of HeLa cells treated with vehicle or 1.8 µM FQI1. Top: Representative image of UV-treated HeLa cells as a positive control. All images were taken at the same intensity. Scale bars: 20 µm.

Figure 2. FQI1 treatment diminished expression of mitotic regulators. A. Schematic of experimental protocol. FQI1 or vehicle was added to HeLa cells during synchronization to the G1/S border using a double thymidine block. Cells were released from the block, including addition of 20 µM of thymidine, for subsequent analyses. **B.** Lysates from cells treated with vehicle or 1.8 µM FQI1 were harvested at release from the G1/S block (0 hours) or 8 hours post release and analyzed for *AURKB* or *CDC20* RNA levels, as normalized to levels of *GAPDH*

bioRxiv preprint doi: https://doi.org/10.1101/665570; this version posted June 11, 2019. The copyright holder for this preprint (which was not certified by peer review) is the author/funder, who has granted bioRxiv a license to display the preprint in perpetuity. It is made available under aCC-BY 4.0 International license.

RNA. Data are plotted relative to the expression from vehicle treated cells at each time point and are representative of 3 independent experiments. **C.** Immunoblots for the indicated proteins in lysates harvested 8 hours post release from a G1/S block, after treatment with increasing concentrations of FQI1. **D.** Quantitation of the protein levels from immunoblots as in C. Protein levels were normalized to those of β-actin. Data are representative of two independent experiments.

Figure 3. RNAi mediated knockdown of LSF reduced expression of mitotic regulators. **A.** Schematic of experimental protocol. siRNAs targeting LSF or a non-expressed target were transfected into HeLa cells at the indicated concentrations, followed by synchronization of cells and release from the G1/S block. **B.** Cells synchronized during treatment with 20 nM of LSF (+) or control siRNA (-) were harvested for RNA at 0 or 8 hours after release from the final G1/S block. *TFCP2* (which encodes LSF), *AURKB*, and *CDC20* RNA levels were measured and normalized to those of *GAPDH* from the same time point. The relative gene expression levels are reported as the fraction of the RNA levels in the control siRNA-treated cells at 0 hours. Data are averages from three independent experiments. **C.** Representative immunoblots of the indicated proteins or protein modifications are shown for lysates harvested at 8 hours post release from the final G1/S block. **D.** Quantification of immunoblots of AURKB and CDC20 (e.g. panel C). Each target protein was normalized to the level of β-actin in the same sample. Error bars represent standard deviation and are representative of three independent experiments.

Figure 4. LSF knockdown in HeLa cells results in mitotic defects. A. Effects of LSF-specific siRNA on synchronized HeLa cells expressing YFP-labeled H2B were analyzed utilizing time-lapse microscopy. Schematic of experimental protocol for panels B-E. **B.** Representative images of cells treated with 20 nM of either control siRNA (top) or LSF siRNA (bottom). Numbers represent the time (in minutes) for one particular cell in the image from nuclear envelope breakdown (designated as time=0 for that cell). **C.** Quantitation of mitotic time from nuclear envelope breakdown (NEB) to anaphase for a population of cells treated with control siRNA or siRNA targeting LSF. Mitotic times (mean time in minutes +/- standard error, n) for 20 nM control siRNA, and 5, 10, or 20 nM LSF siRNA were: 57.9 +/- 2.8, 101; 296 +/- 16, 77; 324 +/-

bioRxiv preprint doi: https://doi.org/10.1101/665570; this version posted June 11, 2019. The copyright holder for this preprint (which was not certified by peer review) is the author/funder, who has granted bioRxiv a license to display the preprint in perpetuity. It is made available under aCC-BY 4.0 International license.

25, 48; and 235 +/- 16, 84; respectively. Error bars indicated standard error of the mean, based on the number of cells analyzed in a single experiment. **D.** Quantitation of cellular events at increasing concentrations of LSF siRNA during the time lapse microscopy, including the percentage of cells that entered mitosis but were delayed with condensed but unaligned chromosomes, and the percentage that exited mitosis, but with multinucleation. The control had neither of these phenotypes among the cells counted (~100 per group). **E.** Bottom: γ-H2AX staining of HeLa cells treated with 20 nM control or LSF siRNA. Top: Representative image of UV-treated HeLa cells as a positive control. All images were captured at the same intensity. Scale bars: 20 µm.

Figure 5. Inhibition of LSF activity induces cellular senescence. **A-B**. HeLa cells treated either with increasing concentrations of FQI1 (0=vehicle control) or with control or LSF siRNA were synchronized using a double thymidine block (protocols in Fig. 2A and 3A, respectively) and then fixed at 8 h after release from the second thymidine block and stained for β-galactosidase activity. Phase contrast images were taken at 20x magnification. Images shown are representative of three independent experiments. Arrows point to examples of cells positive for β-galactosidase. **C-D.** The correlation of increasing LSF siRNA concentrations (C) or increasing FQI1 concentrations (D) with the number β-galactosidase positive cells is depicted as a percentage compared to the control for each individual FQI1 and LSF siRNA concentration. The data reflect analysis of 75 cells per condition in each experiment, averaging over three independent experiments. The Pearson correlation coefficients are indicated.

bioRxiv preprint doi: https://doi.org/10.1101/665570; this version posted June 11, 2019. The copyright holder for this preprint (which was not certified by peer review) is the author/funder, who has granted bioRxiv a license to display the preprint in perpetuity. It is made available under aCC-BY 4.0 International license.

Figure 1

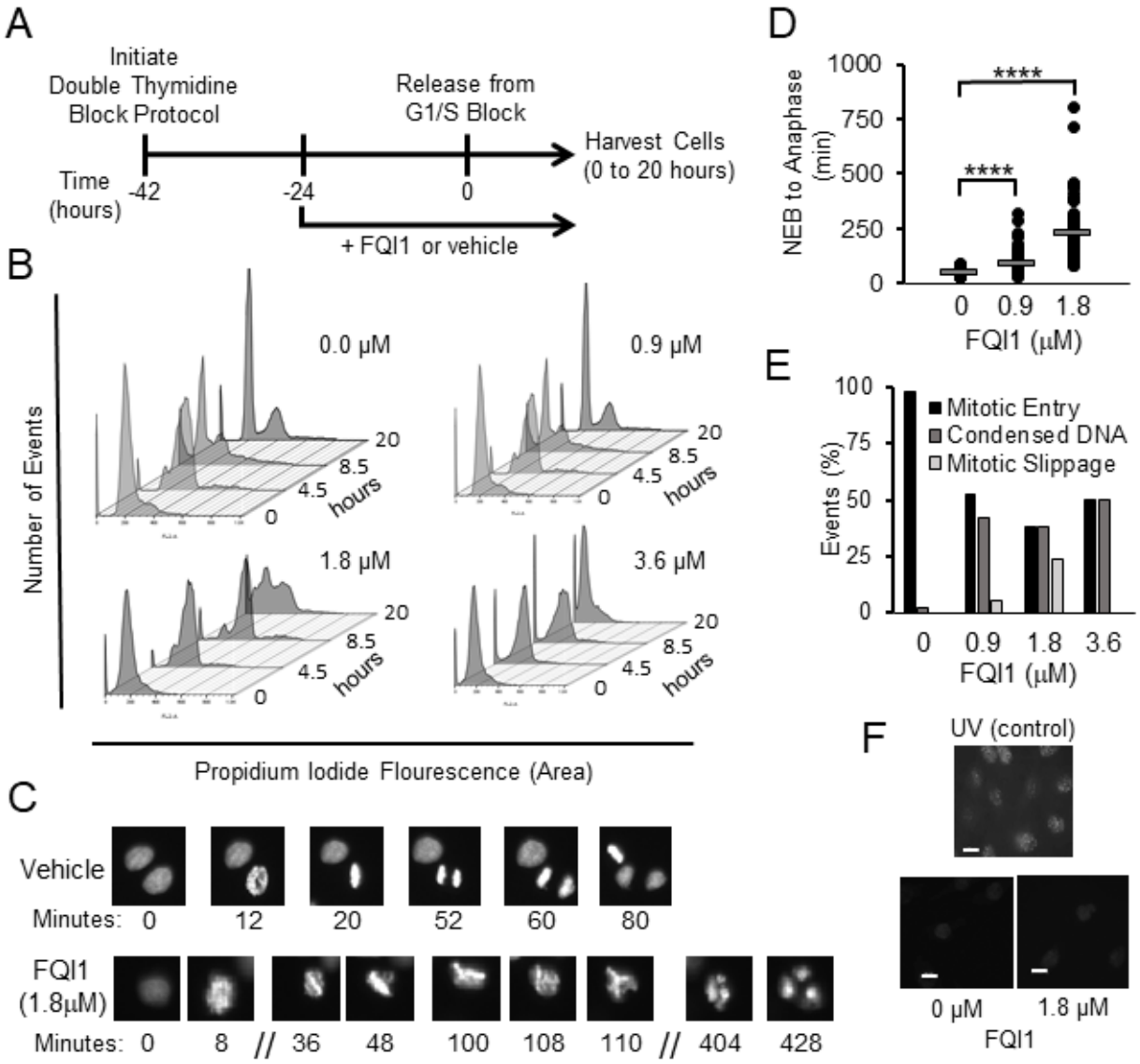

bioRxiv preprint doi: https://doi.org/10.1101/665570; this version posted June 11, 2019. The copyright holder for this preprint (which was not certified by peer review) is the author/funder, who has granted bioRxiv a license to display the preprint in perpetuity. It is made available under aCC-BY 4.0 International license.

Figure 2

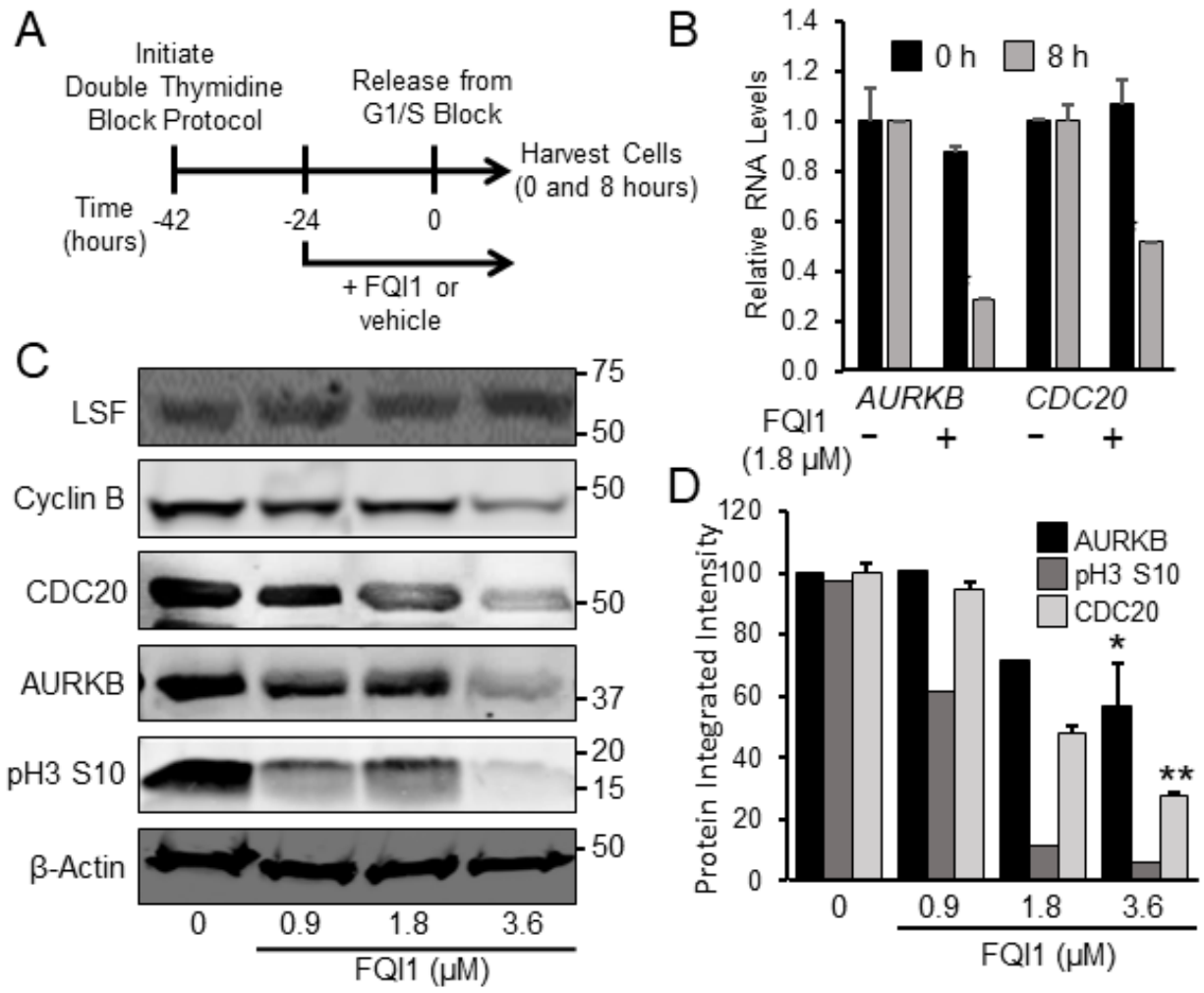

bioRxiv preprint doi: https://doi.org/10.1101/665570; this version posted June 11, 2019. The copyright holder for this preprint (which was not certified by peer review) is the author/funder, who has granted bioRxiv a license to display the preprint in perpetuity. It is made available under aCC-BY 4.0 International license.

Figure 3

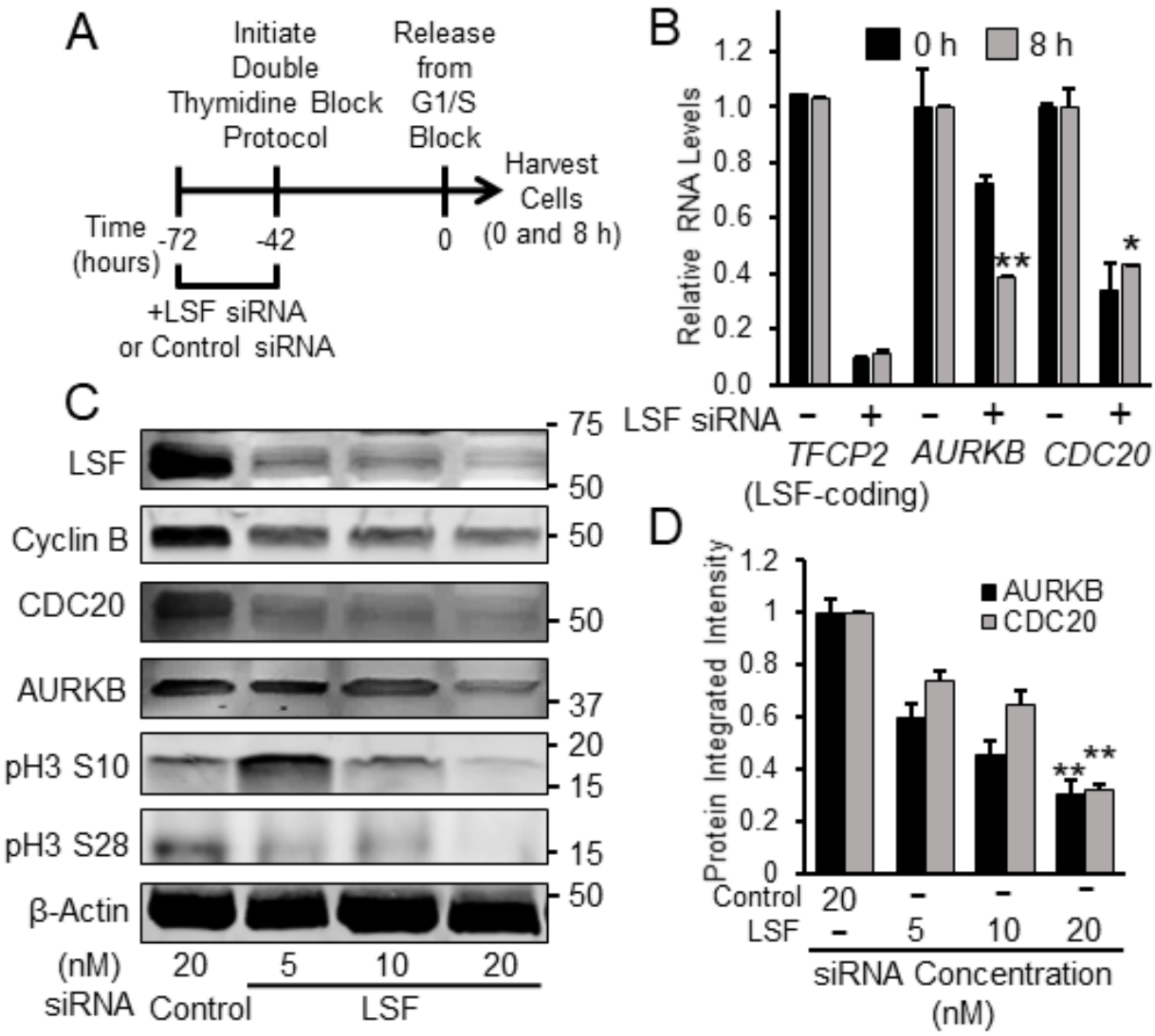

bioRxiv preprint doi: https://doi.org/10.1101/665570; this version posted June 11, 2019. The copyright holder for this preprint (which was not certified by peer review) is the author/funder, who has granted bioRxiv a license to display the preprint in perpetuity. It is made available under aCC-BY 4.0 International license.

Figure 4

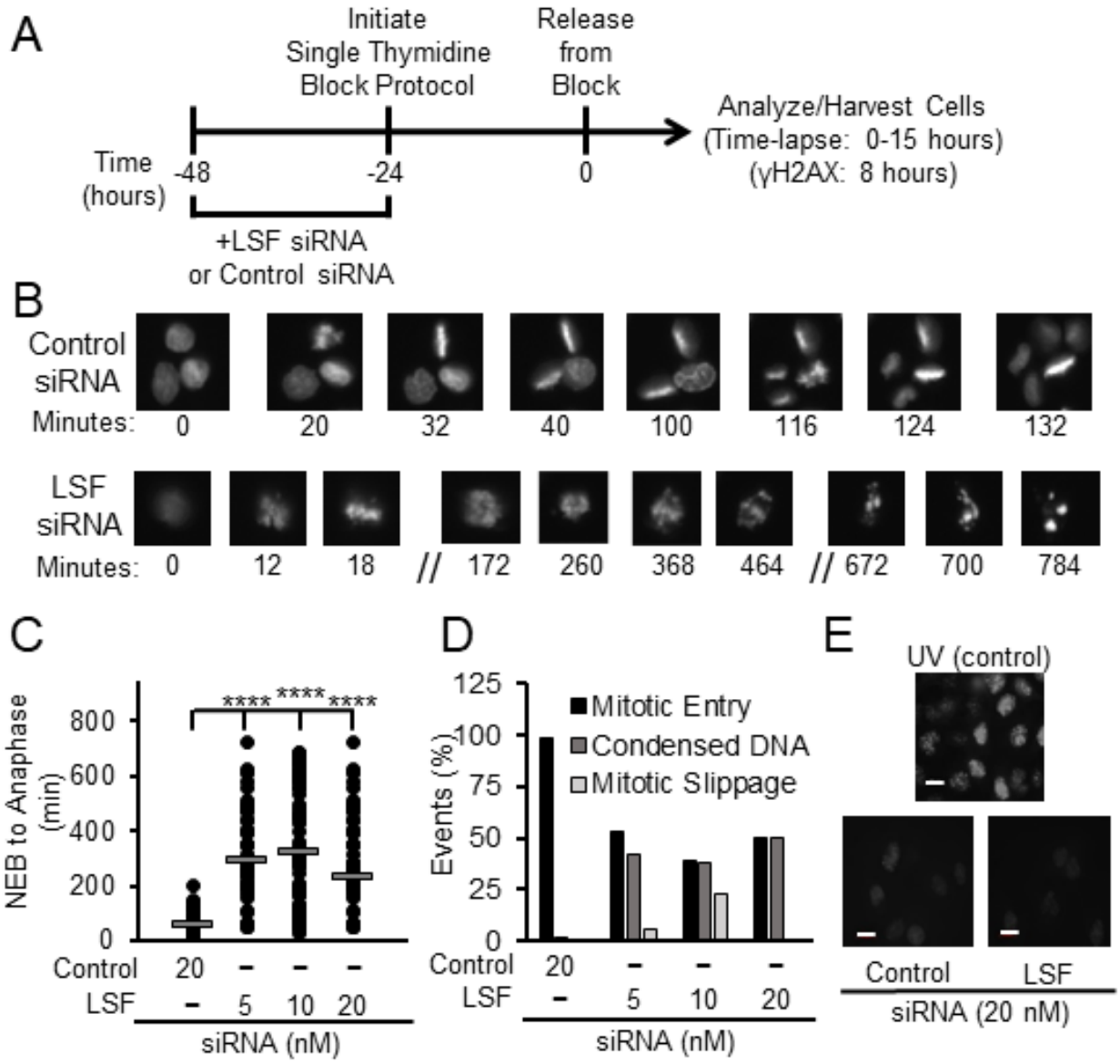

bioRxiv preprint doi: https://doi.org/10.1101/665570; this version posted June 11, 2019. The copyright holder for this preprint (which was not certified by peer review) is the author/funder, who has granted bioRxiv a license to display the preprint in perpetuity. It is made available under aCC-BY 4.0 International license.
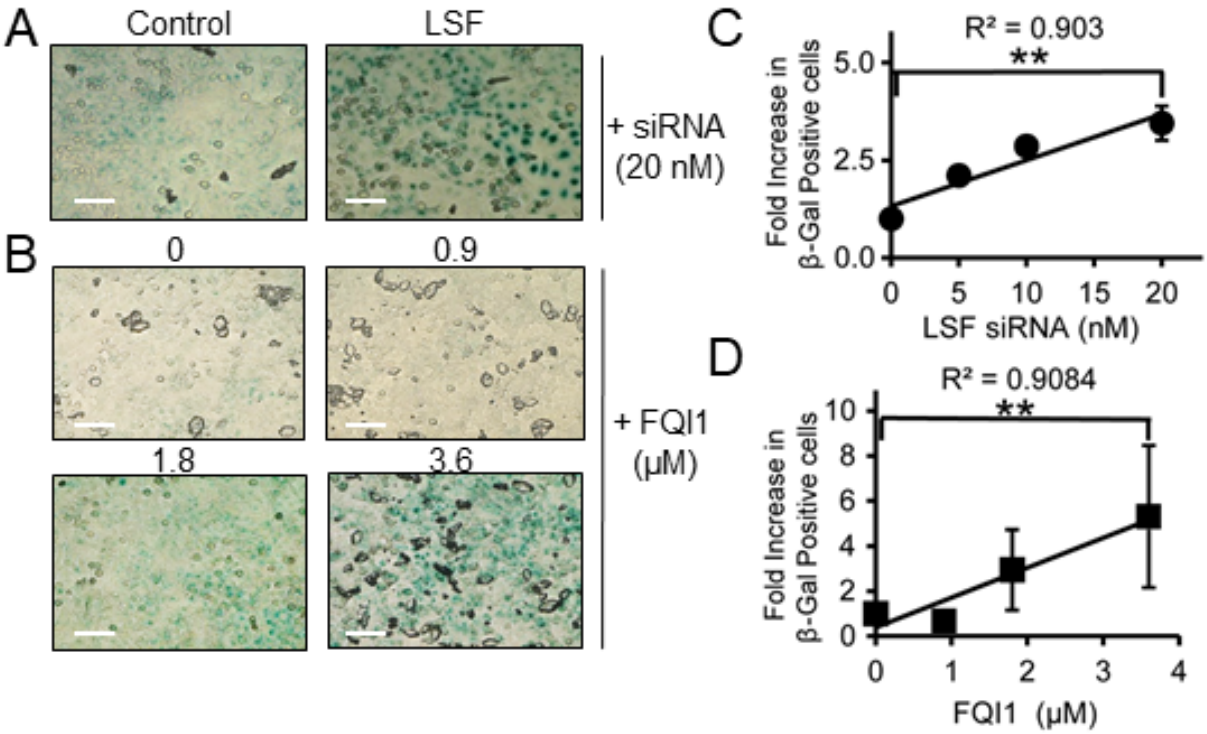
Figure 5